

# NJC

Accepted Manuscript



This is an *Accepted Manuscript*, which has been through the Royal Society of Chemistry peer review process and has been accepted for publication.

*Accepted Manuscripts* are published online shortly after acceptance, before technical editing, formatting and proof reading. Using this free service, authors can make their results available to the community, in citable form, before we publish the edited article. We will replace this *Accepted Manuscript* with the edited and formatted *Advance Article* as soon as it is available.

You can find more information about *Accepted Manuscripts* in the [Information for Authors](#).

Please note that technical editing may introduce minor changes to the text and/or graphics, which may alter content. The journal's standard [Terms & Conditions](#) and the [Ethical guidelines](#) still apply. In no event shall the Royal Society of Chemistry be held responsible for any errors or omissions in this *Accepted Manuscript* or any consequences arising from the use of any information it contains.

## Dihydrogen Phosphate Selective Anion Receptor Based on Acylhydrazone and Pyrazole

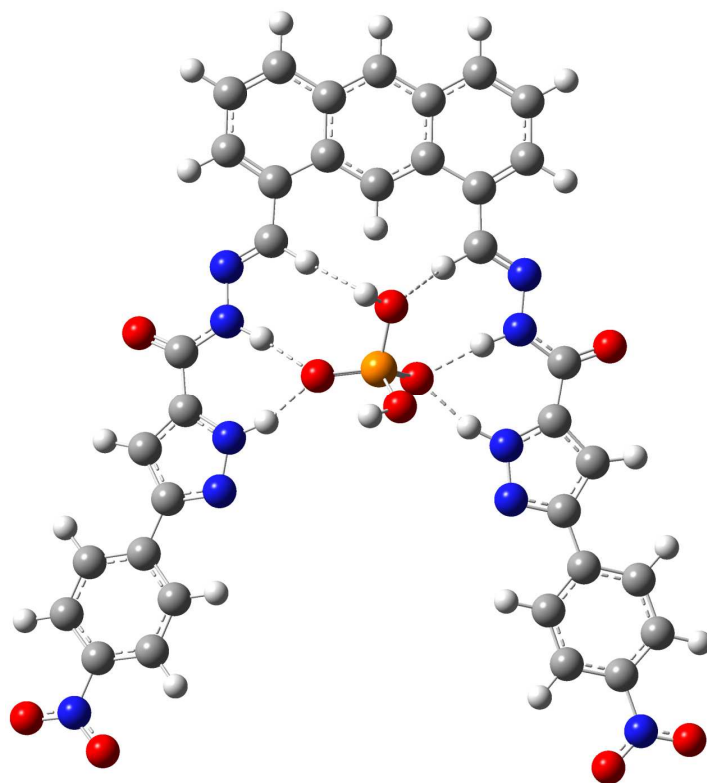
Thiravidamani Senthil Pandian<sup>a</sup>, Yusun Choi<sup>a</sup>,

Venkatesan Srinivasadesikan<sup>b</sup>, Ming-Chang Lin\*<sup>b</sup>, Jongmin Kang\*<sup>a</sup>

<sup>a</sup> Department of Chemistry, Sejong University, Seoul, 143-747, South Korea

<sup>b</sup> Center for Interdisciplinary Molecular Science, Department of Applied  
Chemistry, National Chiao Tung University, Hsinchu 300, Taiwan

Email: kangjm@sejong.ac.kr; [chemmcl@emory.edu](mailto:chemmcl@emory.edu)



## Abstract

A Novel chromogenic anion receptor **1** based on acylhydrazone and pyrazole has been designed and synthesized. Chromogenic anion receptor **1** forms stable 1:1 complexes with dihydrogen phosphate ( $\text{H}_2\text{PO}_4^-$ ) and other halide ( $\text{Cl}^-$ ,  $\text{Br}^-$ ) anions in DMSO solution, as shown by UV-vis, fluorescence and  $^1\text{H}$  NMR spectroscopic experiments. The pyrazole containing host **1** in the optimized geometry of complex has been noted as planar. The planarity of the host with the  $\text{H}_2\text{PO}_4^-$  anion resulted from four strong N-H...O type and two weak C-H...O type H-bonding. In total six H-bondings and the planarity of the host in the complex are responsible for the high binding energy. Addition of an excess of more basic anions ( $\text{F}^-$  and  $\text{CH}_3\text{COO}^-$ ) induces stepwise deprotonation, an event signalled by the appearance of a bright yellow color. The intensity of fluorescence spectrum increases when hydrogen bonding occurs and decreases when deprotonation occurs which is evidenced by fluorescence titrations.

## Introduction

Phosphate-binding receptors have become a highly favourable target in molecular recognition chemistry due to the importance of biological and environmental role of phosphate. For example, phosphate is an essential component of chemotherapeutic and antiviral drugs.<sup>1-3</sup> Moreover, phosphate is becoming a main water pollutant in many countries, and causes serious environmental problem.<sup>4-7</sup> Therefore, several systems designed to selectively coordinate phosphate were reported.<sup>8-10</sup>

As anions display wide range of geometries, design and synthesis of artificial receptors that exhibit high binding affinity and selectivity to a targeted anion still remain a great challenge. Among various noncovalent interactions, hydrogen-bonding interactions are particularly useful and effective in this regard. To achieve high binding affinity and good selectivity, hydrogen bonding moieties are arranged in space in a rigid and convergent manner. In addition, receptors bearing multiple hydrogen bonding moieties have been shown to be useful to promote cooperative binding, which would result in enhanced binding affinity.<sup>11-12</sup> Previously we have achieved selective and cooperative hydrogen bonding for dihydrogen phosphate utilizing acylhydrazone and indole.<sup>13</sup> Recently, we also found that similar selective and cooperative hydrogen bonding for dihydrogen phosphate could be achieved by introducing pyrazole group instead of the indole group. From modeling, we found that six H-bondings resulted from four strong N-H...O type and two weak C-H...O type H-bonding and the planarity of the host in the complex are responsible for the high binding energy. Here we'd like to report the synthesis and the anion binding phenomena of receptor **1**. The binding phenomena of receptor **1** could be monitored by UV-vis, fluorescence and <sup>1</sup>H NMR spectra.

## Experimental Section

### Materials

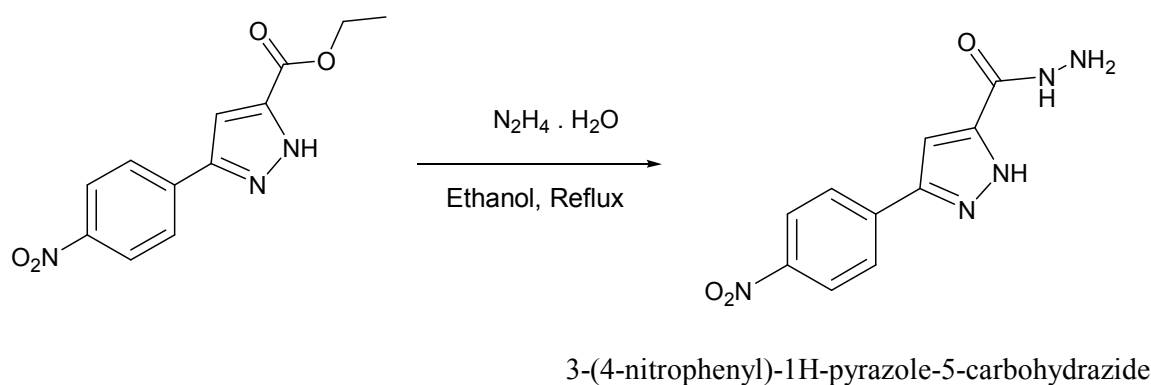
tetra-n butylammonium hydroxide (TBAOH), tetra-n-butylammonium fluoride (TBAF), tetra-n-butylammonium dihydrogen phosphate (TBAH<sub>2</sub>PO<sub>4</sub>), tetra-n-butylammonium acetate (TBAA), and tetra-n-butylammonium bromide (TBABr), tetra-n-butylammonium chloride (TBACl) tetra-n butylammonium hydrogen sulphate (TBAHSO<sub>4</sub>), were purchased from Sigma-Aldrich Chemical Co., Inc., and used as received.

### Measurements

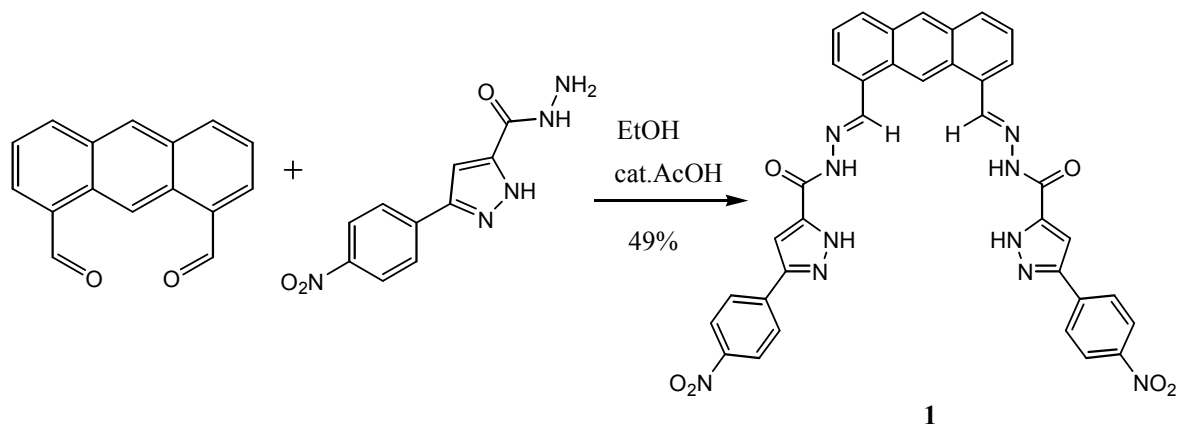
.Absorption spectra were recorded using a biochrom Libra S70 spectrophotometer (Biochrom Ltd, England). NMR spectra were recorded using a BRUKER spectrometer operated at 500 MHz. ESI MS spectra were obtained using a JMS 700 (Jeol, Japan) double focusing magnetic sector mass spectrometer. All measurements were carried out at room temperature (298 K).

### Synthesis

3-(4-nitrophenyl)-1*H*-pyrazole-5-carbohydrazide was prepared according to the previous literature protocol.<sup>14</sup>



Receptor **1** was synthesized by reacting anthracene-1,8-dicarbaldehyde<sup>15</sup> and 3-(4-nitrophenyl)-1*H*-pyrazole-5-carbohydrazide in ethanol using acetic acid as catalyst at a yield of 49 %.



### 3-(4-nitrophenyl)-1*H*-pyrazole-5-carbohydrazide

A mixture of 0.285g (1.09 mmol) ethyl 3-(4-nitrophenyl)-1*H*-pyrazole-5-carboxylate and 0.462 mL (0.0148mmol) of hydrazine hydrate in 10 mL of ethanol was refluxed for 36 h then cooled. The solid collected by filtration, washed with water, and dried in vacuo, gave the desired product (0.269g, 74.3%)  $^1\text{H}$  NMR (500 MHz, DMSO- $d_6$ )  $\delta$  14.01 (br, 1H),  $\delta$  9.84 (s, 1H),  $\delta$  8.31 (d,  $J = 8.5$ , 2H),  $\delta$  8.02 (d,  $J = 8.5$ , 2H),  $\delta$  7.35 (s, 1H),  $\delta$  4.54 (br, 2H)  $^{13}\text{C}$  NMR (500 MHz, DMSO- $d_6$ )  $\delta$  158.44 148.60 146.64 139.47 137.92 125.91 124.34 102.77

### Receptor 1

Anthracene-1,8-dicarbaldehyde (70 mg, 0.3 mmol), 3-(4-nitrophenyl)-1*H*-pyrazole-5-carbohydrazide (147 mg, 0.6 mmol) and three drops of acetic acid were dissolved in 25 ml ethanol. The above mixed solution was heated to reflux for overnight and then cooled to room temperature. The formed precipitate was filtered off and washed with ethanol to afford (101 mg, 49%) of receptor.  $^1\text{H}$  NMR (500 MHz, DMSO- $d_6$ )  $\delta$  11.28 (s, 1H),  $\delta$  9.46 (s, 2H),  $\delta$  8.77 (s, 1H),  $\delta$  8.25 (d,  $J = 8.5$ , 2H),  $\delta$  8.03 (d,  $J = 6.9$ , 8H),  $\delta$  7.82 (br, 2H),  $\delta$  7.69 (t,  $J = 7.5$ , 2H),  $\delta$  7.39 (br, 2H)  $^{13}\text{C}$  NMR (500 MHz, DMSO- $d_6$ )  $\delta$  147.55 146.39 131.16 130.29 129.89 128.54.92 127.19 125.69 125.32 123.90 123.54 104.63 HRMS (FAB, double focusing mass sector) calcd for  $\text{C}_{36}\text{H}_{24}\text{O}_6 \text{N}_{10} \text{Na}$   $[\text{M}+\text{Na}]^+$ : 715.1778,

found: 715.1779

## Results and discussion

### Interactions with Dihydrogen Phosphate

The ability of receptor **1** to recognize dihydrogen phosphate was first studied in DMSO using UV-vis titration spectra. Receptor **1** displayed absorption bands at 268, 299, 407, and 433 nm. Upon addition of increasing amounts of  $\text{H}_2\text{PO}_4^-$ , moderate increases and decreases in absorption at different wavelengths (Figure 1), and multiple isosbestic points were observed at 285, 306, 380, 398, 414, 427, and 438 nm, suggesting typical hydrogen bonding complex formation between receptor **1** and dihydrogen phosphate.

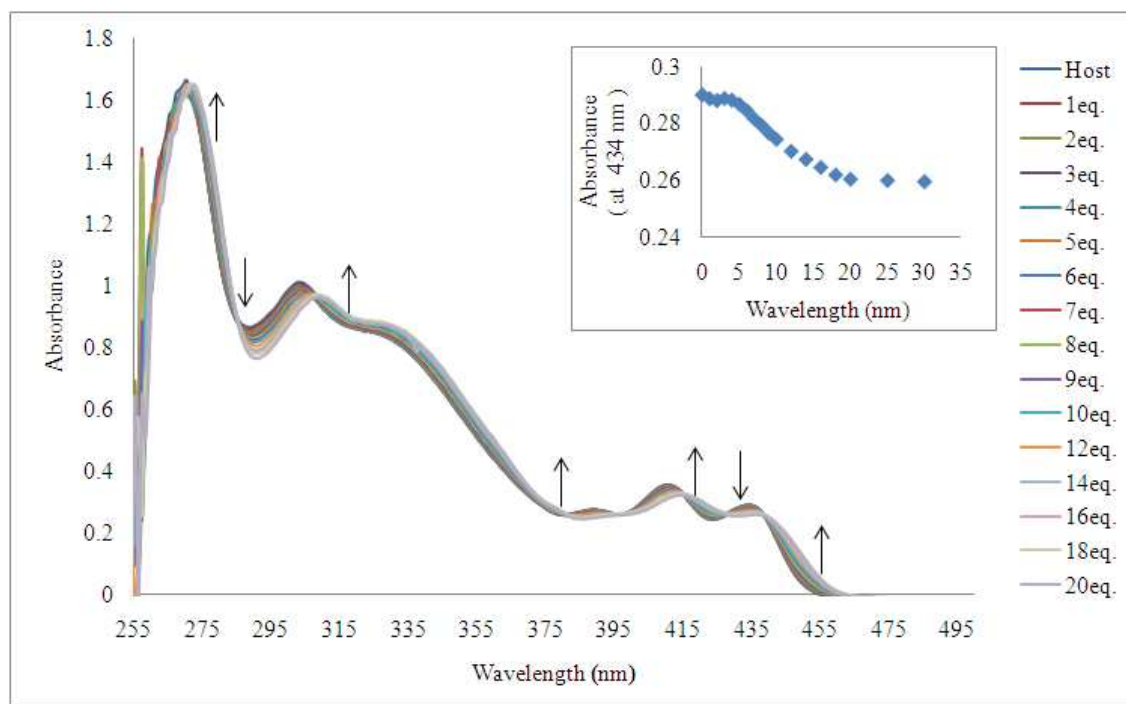


Figure 1. Family of spectra recorded over the course of titrating a 20  $\mu\text{M}$  DMSO solution of the receptor **1** with increasing amounts of tetrabutylammonium dihydrogen phosphate

Receptor **1** showed strong fluorescence emission spectrum in DMSO as expected. The excitation wavelength was 394 nm and emission wavelengths were 422, 452 and 475 nm. The

intensity of the emission spectrum from 20  $\mu\text{M}$  solution of the receptor **1** gradually increased as the concentration of tetrabutylammonium dihydrogen phosphate salts was increased (1–23 equiv.), which also indicates the association between the receptor **1** and dihydrogen phosphate. (Figure 2)

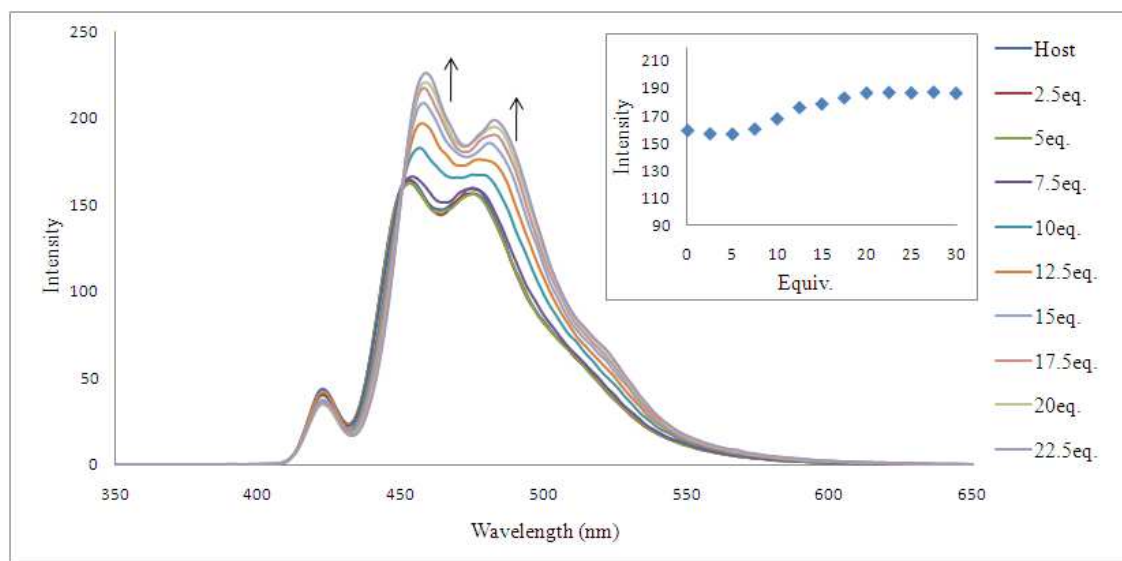


Fig. 2 The change of fluorescence spectra over the course of titration of 20  $\mu\text{M}$  DMSO solutions of the receptor **1** when tetrabutylammonium dihydrogen phosphate was added. The change of fluorescence of intensity measured at 475 nm.

Hydrogen bond formation was also confirmed by  $^1\text{H}$  NMR titration. In the  $^1\text{H}$  NMR of receptor **1**, not only amide N-H and pyrazole N-H peaks but also imine C-H peak is broad probably due to slow rotation of two pyrazole arm. When dihydrogen phosphate was added, two N-H peaks showed intense broadening and the imine C-H peak ( $\text{H}_i$ ) showed a downfield shift (Figure 3). We believe that these phenomena were caused by a slow equilibrium between receptor **1** and dihydrogen phosphate as well as the complexation of added dihydrogen phosphate by receptor **1** through amide N-H, pyrazole N-H, and imine C-H

hydrogen bond formation.<sup>16-18</sup> Furthermore, anthracene 9-H(H<sub>9</sub>) showed upfield shift. In fact, two effects are expected as a result of hydrogen bond formation between receptor **1** and the anion. A through-bond propagation increases electron density in the anthracene ring, which causes a shielding effect and promotes an upfield shift (ii) A through-space effect increases a polarization of C–H bonds, which causes deshielding and promotes a downfield shift. In this case, the through-bond propagation dominates, and an upfield shift is observed for the anthracene 9-H peak.

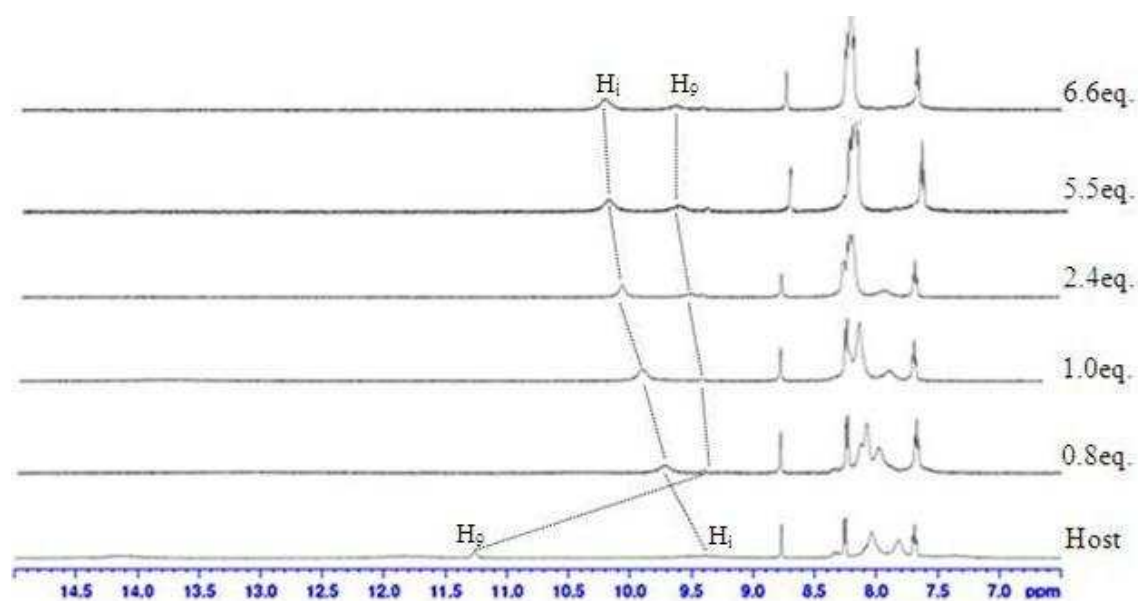


Figure 3. <sup>1</sup>H NMR spectra of 2 mM of receptor **1** containing increasing amounts of tetrabutylammonium dihydrogen phosphate (0 –6.6 equiv.) in DMSO-d<sub>6</sub>

The stoichiometry between receptor **1** and dihydrogen phosphate was determined to be 1:1 using a UV-vis Job plot in DMSO-d<sub>6</sub> (Figure 4). A Benesi–Hildebrand plot<sup>19</sup> by use of change at 433 nm in UV-vis spectrum and 475 nm in fluorescence spectrum gave the association constants for dihydrogen phosphate. The calculated association constants for dihydrogen phosphate were  $1.2 \times 10^4$  by UV-vis titration and  $1.1 \times 10^4$  by fluorescence titration.

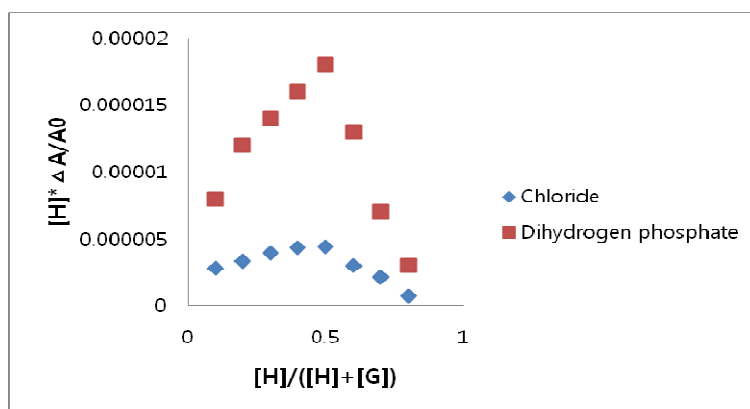


Figure 4. Job plots of receptor **1** with tetrabutylammonium dihydrogen phosphate and tetrabutylammonium chloride obtained by UV-vis spectrum in DMSO

### Interactions with halides

The abilities of receptor **1** to recognize halides were also studied in DMSO using UV-vis titration spectra. When the amount of chloride was increased, a moderate decrease in absorbance was observed throughout most of the spectrum. However, moderate increases in absorbance were observed above 443 nm with an isosbestic point at this wavelength (Figure 5), suggesting typical hydrogen bonding complex formation between receptor **1** and chloride. The existence of isosbestic point for UV-vis titrations of receptors **1** with chloride suggests a 1:1 complexation, and this was also confirmed by Job's plot analysis (Figure 4).

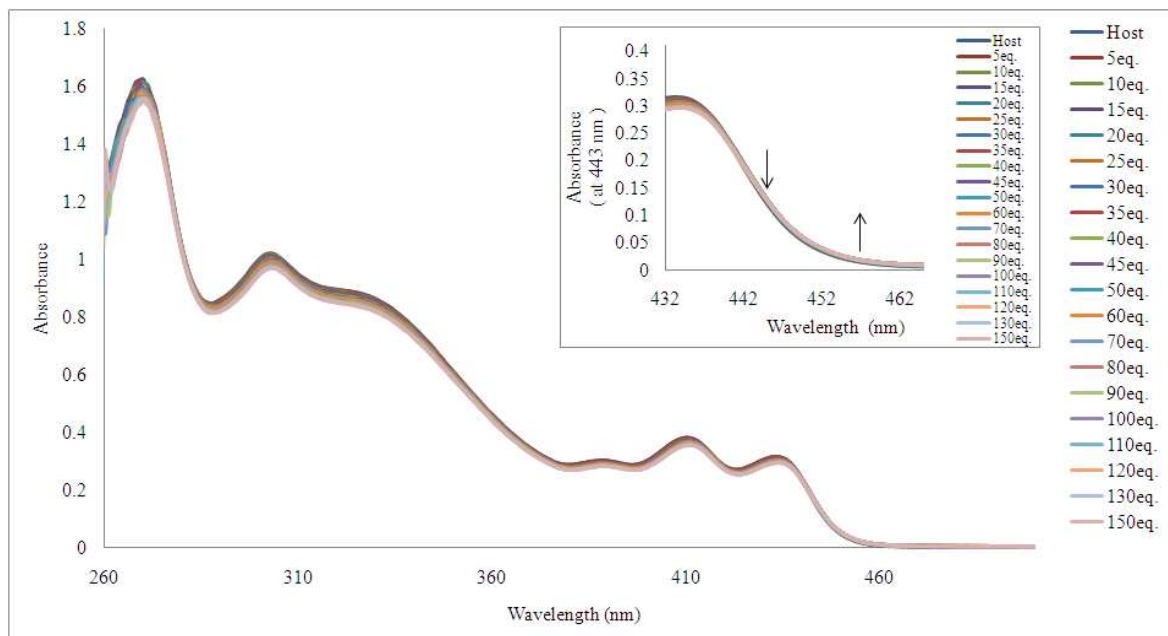


Figure 5. A family of spectra recorded over the course of titrating a 20  $\mu\text{M}$  DMSO solution of receptor **1** with increased amounts of tetrabutylammonium bromide.

In fluorescence titration with chloride, the intensity of the emission spectrum gradually increased as the concentration of tetrabutylammonium chloride salts was increased (1–150 equiv.), which also indicates hydrogen bonding between the receptor **1** and chloride (Figure 6).

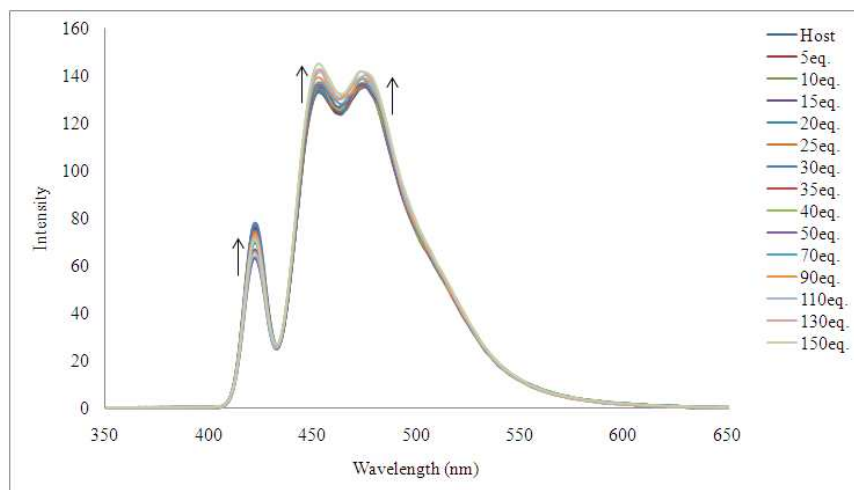


Fig. 6 The change of fluorescence spectra over the course of titration of 20  $\mu\text{M}$  DMSO solutions of the receptor **1** when tetrabutylammonium chloride was added.

The association constants calculated for chloride were  $8.0 \times 10^2$  for UV-Vis titration and  $5.7 \times 10^2$  for fluorescence titration. Other halides such as bromide showed similar behaviors to chloride; calculated binding constants for other anions are summarized in Table 1.

Table 1 Association constants ( $\text{M}^{-1}$ ) of receptors **1** with various anions in DMSO

Anion	UV	Fluorescence
$\text{H}_2\text{PO}_4^-$	$1.2 \times 10^4$	$1.1 \times 10^4$
$\text{HSO}_4^-$	$1.1 \times 10^3$	$1.2 \times 10^3$
$\text{Cl}^-$	$8.0 \times 10^2$	$5.7 \times 10^2$
$\text{Br}^-$	$5.3 \times 10^2$	$5.2 \times 10^2$
$\text{CH}_3\text{COO}^-$	DP	DP
$\text{F}^-$	DP	DP

DP - deprotonation

The selective sensing ability of receptor **1** for tetrahedral shaped anions such as dihydrogen phosphate and hydrogen sulfate could be seen from fluorescence intensity change with binding anions. No significant fluorescence intensity changes were observed on the addition

of 22 equiv of haides such as chloride and bromide. (Figure 7) This result shows that receptor **1** has optimum geometry for dihydroegn phosphate.

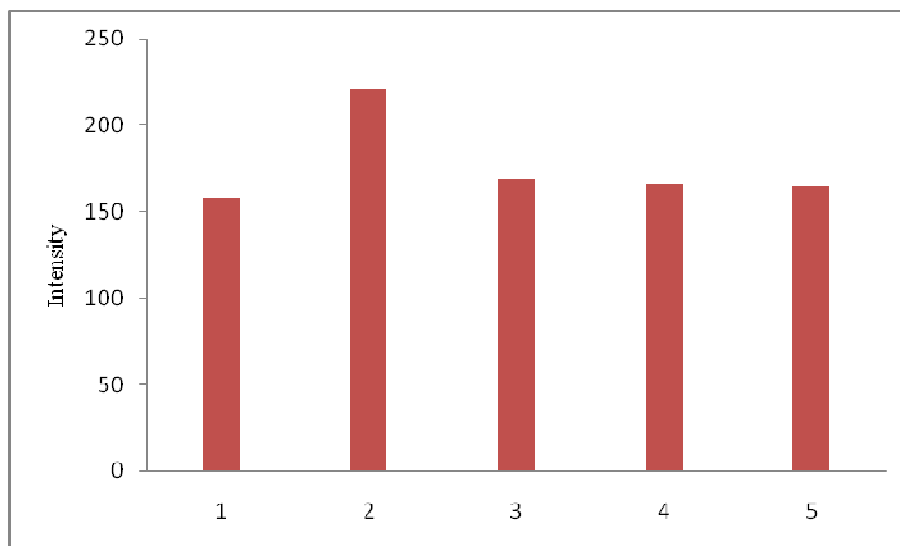


Figure 7. Fluorescence intensity changes of **1** (20  $\mu\text{M}$ ) upon the addition of various anions (22 equiv) in DMSO at  $\lambda_{\text{ex}} = 460 \text{ nm}$  1, Host **1** alone; 2, H<sub>2</sub>PO<sub>4</sub><sup>-</sup>; 3, HSO<sub>4</sub><sup>-</sup>; 4, Cl<sup>-</sup>; 5, Br<sup>-</sup>

### Interactions with hydroxide, fluoride and acetate

In order to discriminate between H-bonding and deprotonation, UV-vis titration of receptor **1** with tetrabutylammonium hydroxide was carried out (Figure 8). Changes in the absorbance spectra in the presence of hydroxide were clearly different from those observed for dihydrogen phosphate. Furthermore, only one isosbestic points was observed at 362 nm, which differed from those observed in the presence of dihydrogen phosphate. In addition, UV-vis spectral changes upon adding excessive fluoride were almost identical to those induced by hydroxide.

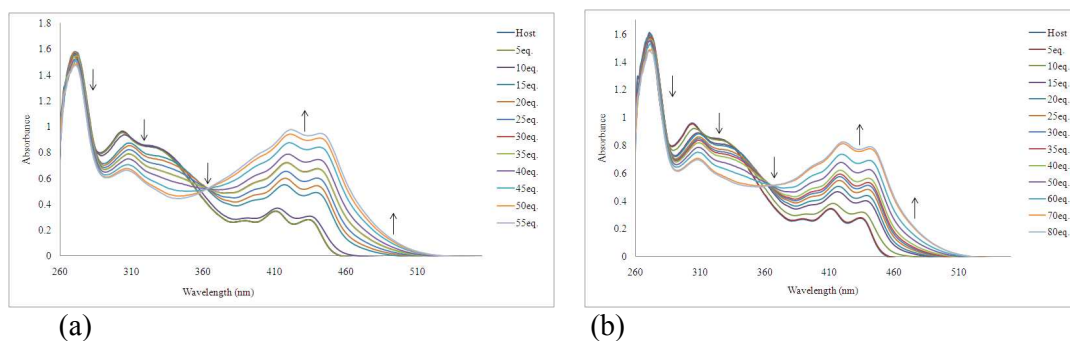


Figure 8. Family of UV-vis spectra recorded over the course of titrating a 20  $\mu\text{M}$  DMSO solution of receptor **1** with increasing amounts of tetrabutylammonium hydroxide (a) and tetrabutylammonium fluoride (b)

In UV-vis titration with acetate, similar phenomenon was observed with isosbestic point at 343 nm. In fluorescence titration with acetate, the intensity of the emission spectrum from 20  $\mu\text{M}$  solution of the receptor **1** gradually decreased as the concentration of tetrabutylammonium acetate salts was increased (1–80 equiv.). The decrease of fluorescence intensity was also observed with hydroxide. (see supporting information) Therefore, it could be concluded that only deprotonation occurred with acetate. It was not easy to figure out which hydrogen is deprotonated first between pyrazole N-H( $\text{H}_{29}$ ,  $\text{H}_{57}$ ) and amide N-H( $\text{H}_{45}$ ,  $\text{H}_{72}$ ) from the receptor **1** as both peaks are too broad. Therefore we tried  $^1\text{H}$  NMR titration of 3-(4-nitrophenyl)-1H-pyrazole-5-carbohydrazide, which showed pyrazole peak and amide peak clearly. When we add 0.5 equivalents of tetrabutylammonium fluoride, we observed pyrazole peak was disappeared first (Figure 9). From this experiment, we suggest that pyrazole N-H( $\text{H}_{29}$ ,  $\text{H}_{57}$ ) would be deprotonated first from the receptor **1** although we cannot see the deprotonation phenomena of receptor **1** clearly through  $^1\text{H}$  NMR.

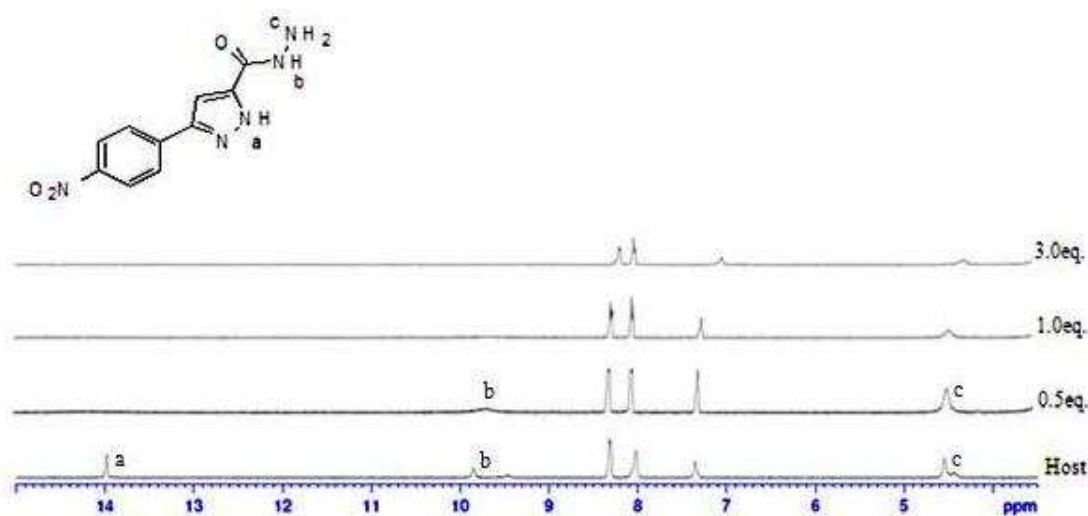


Figure 9.  $^1\text{H}$  NMR spectra of 2 mM of 3-(4-nitrophenyl)-1H-pyrazole-5-carbohydrazide containing increasing amounts of tetrabutylammonium fluoride (0 –3 equiv.) in  $\text{DMSO-d}_6$

Figure 10 shows color change of solutions of receptor **1** after adding various anions in DMSO. Color changes from light green to purple or intense yellow were observed in the presence of hydroxide, fluoride or acetate whereas dihydrogen phosphate did not induce any color change. UV-vis titration results and these color changes suggest that deprotonation events occurred by hydroxide, fluoride and acetate but hydrogen bonding occurs between dihydrogen phosphate and receptor **1**.

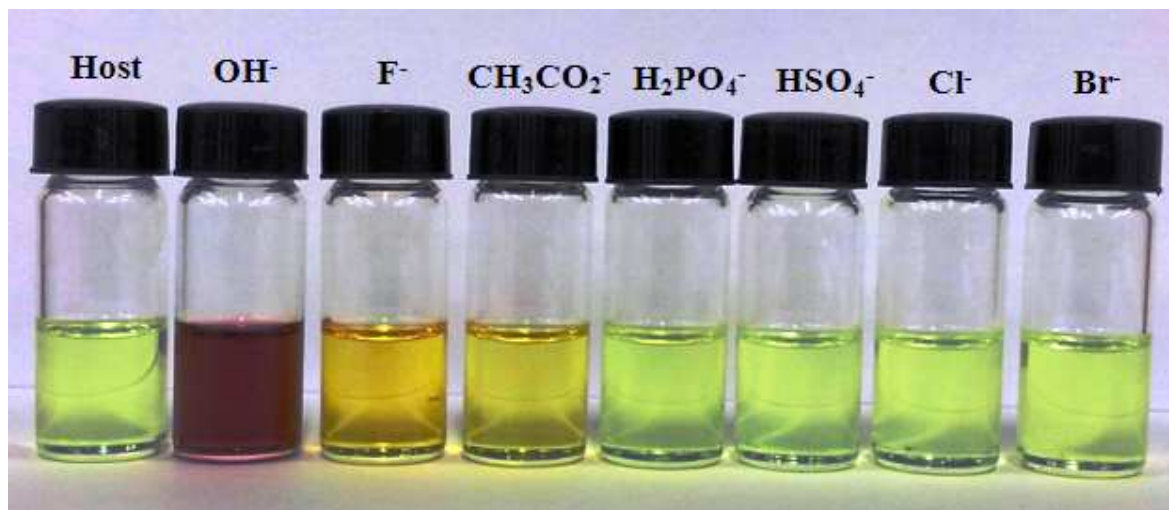


Figure 10. Color changes of receptor 1 at 100  $\mu\text{M}$  in DMSO when treated with 80 equivalents of various anions.

The other anions did not induce any color changes even when added in excess. The examples of selective sensing acetate from dihydrogen phosphate are relatively limited due to similarity of their basicity. However, they were able to be differentiated by considering the different color responses observed.

### Binding Energy Studies

In the present study the computational modeling using the DFT (density functional theory) method has been carried out for the pyrazole containing receptor with dihydrogen phosphate,  $\text{Br}^-$ ,  $\text{Cl}^-$  and  $\text{HSO}_4^-$  anion complexes. The common hybrid B3LYP method is chosen as for this study.

The B3LYP hybrid functional is consisting of Becke's exchange functional, the Lee-Yang-Parr correlation functional, and a Hartree-Fock exchange term. The DFT has been

successfully used to study hydrogen-bonded complexes,<sup>20</sup> even for the most weakly bounded systems.<sup>21</sup> The calculated binding energy is corrected for basis set super position error (BSSE) using the counter poise method.<sup>22</sup> The experimental binding constant of newly synthesized compound shows almost similar to the previously reported receptors,<sup>13</sup> which was unexpected because the present receptor here seems to be formed possibly four strong N-H---O and two weak C-H---O types H-bonding. So, we have decided to investigate the binding poses more accurately using the state-of-the-art density functional theory. Figure 11 shows the optimized structure of host and their  $\text{H}_2\text{PO}_4^-$  complex optimized at the B3LYP level<sup>23-26</sup> using the 6-31g (d) basis set. The binding energies of experimental and theoretical values were reported in Table 2.

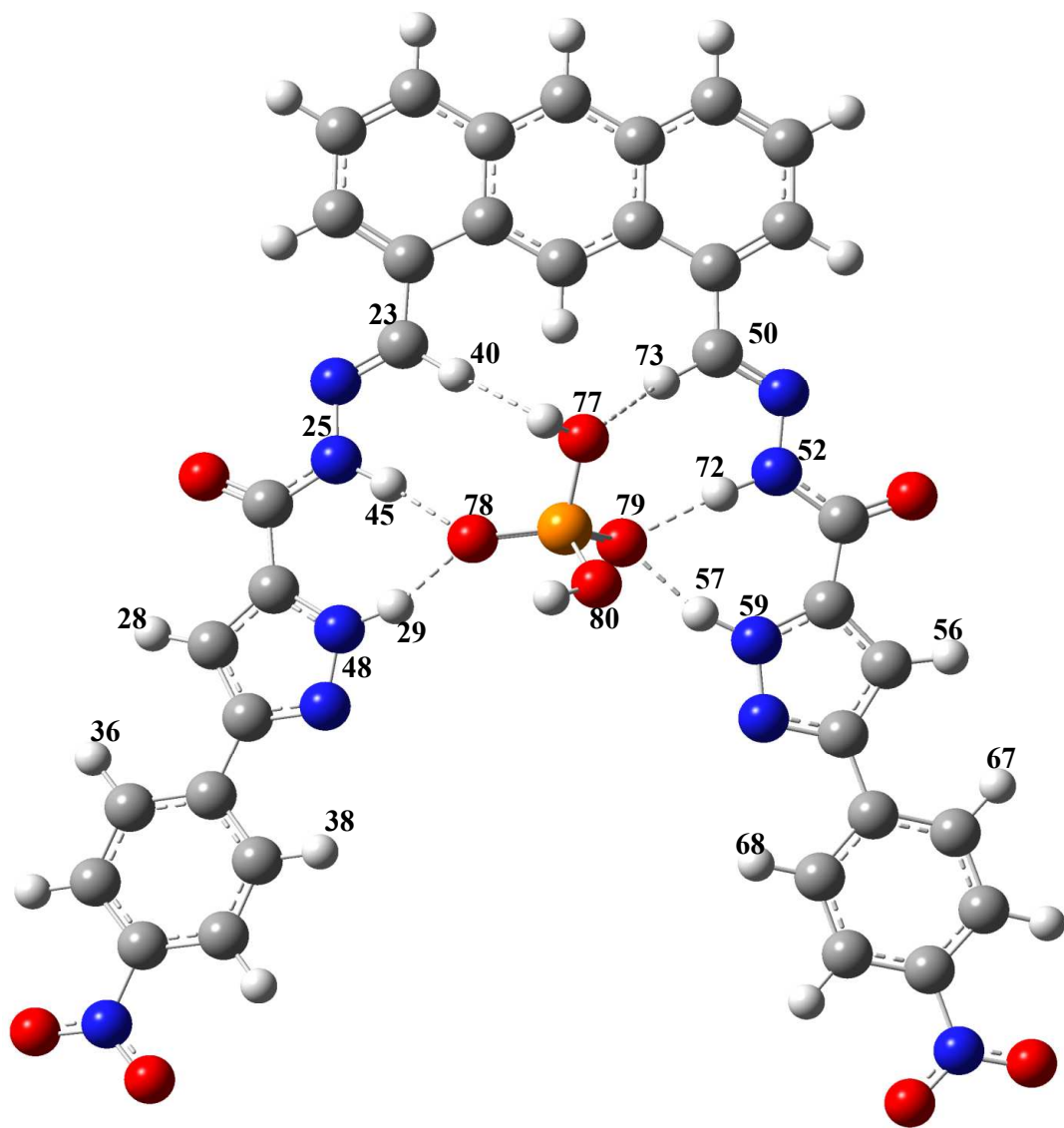


Figure 11. Most stable structure for Host.H<sub>2</sub>PO<sub>4</sub><sup>-</sup> complex in solvent phase (DMSO as a solvent) optimized using B3LYP/6-31g(d) in Gaussian 09. Dashed lines denote the hydrogen bonds (strong and weak). See Table 3 for geometrical parameters and Mulliken charges. Atom numbering included. Atom colors: Grey- Carbon; Red- Oxygen; Blue- Nitrogen; White- Hydrogen; Orange- Phosphorus

Table 2. Experimental and Computational Binding Energies (BE) for Host with anion complexes<sup>a</sup>

Anions	BE	
	exp (UV)	calc (DFT)
H <sub>2</sub> PO <sub>4</sub> <sup>-</sup>	-5.56	-24.96
HSO <sub>4</sub> <sup>-</sup>	-4.15	-16.27
Cl <sup>-</sup>	-3.96	-13.04
Br <sup>-</sup>	-3.71	-11.69

<sup>a</sup>Units are in kcal/mol. Experimental binding energy is derived from UV binding constant. DFT calculations are performed at (B3LYP/6-31G(d)) using a polarizable continuum model in DMSO. The basis set superposition error is corrected.

Table 3. Charges and Geometries of Host and their  $\text{H}_2\text{PO}_4^-$  complex (cx).

Mulliken atomic charges ( $e$ )	cx	Host
	H <sub>40</sub>	0.1669 0.167
	H <sub>15</sub>	0.1617 0.1578
	H <sub>73</sub>	0.1914 0.167
	H <sub>29</sub>	0.4084 0.3833
	H <sub>45</sub>	0.4185 0.3632
	H <sub>57</sub>	0.4174 0.3833
	H <sub>72</sub>	0.4255 0.3632
Heavy atom distance (Å)	C <sub>23</sub> -O <sub>77</sub>	3.848
	C <sub>7</sub> -O <sub>77</sub>	3.774
	C <sub>50</sub> -O <sub>77</sub>	3.474
	N <sub>48</sub> -O <sub>78</sub>	2.752
	N <sub>25</sub> -O <sub>78</sub>	2.874
	N <sub>59</sub> -O <sub>79</sub>	2.761
	N <sub>52</sub> -O <sub>79</sub>	2.866
H-bond distance (Å)	H <sub>40</sub> ...O <sub>77</sub>	2.771
	H <sub>15</sub> ...O <sub>77</sub>	2.939
	H <sub>73</sub> ...O <sub>77</sub>	2.521
	H <sub>29</sub> ...O <sub>78</sub>	1.758
	H <sub>45</sub> ...O <sub>78</sub>	1.848
	H <sub>57</sub> ...O <sub>79</sub>	1.762
	H <sub>72</sub> ...O <sub>79</sub>	1.838
Bond angle (deg)	C <sub>23</sub> H <sub>40</sub> O <sub>77</sub>	168.5
	C <sub>7</sub> H <sub>15</sub> O <sub>77</sub>	134.4
	C <sub>50</sub> H <sub>73</sub> O <sub>77</sub>	145.5
	N <sub>48</sub> H <sub>29</sub> O <sub>78</sub>	160.9
	N <sub>25</sub> H <sub>45</sub> O <sub>78</sub>	172.5
	N <sub>59</sub> H <sub>57</sub> O <sub>79</sub>	133.2
	N <sub>52</sub> H <sub>72</sub> O <sub>79</sub>	174.0

The experimental binding energy is derived from binding constant (UV experiments). For the effort of solvent effect the DMSO is considered using the PCM (polarizable continuum model).<sup>27</sup> The binding energy calculation and computational details have been described in supporting information. All calculations have been computed by using the Gaussian 09 suite

of programs.<sup>28</sup>

To obtain the complex structure, several geometries have been considered for optimization. Here, we chose the lowest-energy structure as a representative one. All geometries of the host, guest and complex have been optimized without any stringent optimization criteria. We could not perform the second derivatives due to the sized the system and the limitation of computational resources. We assume that the experimental binding energies should correlate with the calculated binding energy value (See Table 2). When we compare the calculated binding energy with the experimental binding energy, we have noted the difference between the theory and experiment. The divergence is not unexpected due to the crude solvation model used in the theoretical calculation and the host-anion complex interactions are rather complicated. The chronological order of binding energies derived from the theoretical calculation for host-anion complexes is consistent with the experimental results. (See Table 2). Further, the results have been focused on host.H<sub>2</sub>PO<sub>4</sub><sup>-</sup> complex due to the large binding energy and specific binding property towards pyrazole receptor in the current study.

Theoretically the calculated structure contains all experimentally observed H-bonding elements (Fig. 11). The remarkable result of the computed binding configuration of the host-H<sub>2</sub>PO<sub>4</sub><sup>-</sup> complex reveals that all the N-H protons have acted as a donor towards the H<sub>2</sub>PO<sub>4</sub><sup>-</sup>. Overall, four N-H...O type H-bondings have been observed in the host-H<sub>2</sub>PO<sub>4</sub><sup>-</sup> complex. Moreover, two additional weak C-H...O type H-bonding have also been observed. The newly introduced pyrazole group instead of the indole group in our previous report shows the strong binding with H<sub>2</sub>PO<sub>4</sub><sup>-</sup> due to the strong four N-H...O type H-bonding. And, the pyrazole containing host in the optimized geometry of complex has been interestingly noted to be planar, which is not the case in the indole containing host optimized geometry of the

complex in our previous report<sup>13</sup>. The planarity of the host with a strong H-bonding has produced the highest binding energy for the presently investigated pyrazole containing host complex. The bond angle of  $\angle N_{48}H_{29}O_{78}$  is observed to be  $160.9^\circ$  in the complex. All hydrogens in the cage of the pyrazole containing host pointing towards the oxygen of  $H_2PO_4^-$  anion and have formed the H-bonding in complex. We have also attempted to optimize the geometry to form the H-bonding with O-H<sub>83</sub> in  $H_2PO_4^-$  anion with N<sub>49</sub> in pyrazole ring. But, the optimized results give the similar type of geometry shown in Figure 11 of the present study, due to the long distance between O-H<sub>83</sub> and N<sub>49</sub>, 4.834 Å, which is too far for H-bonding. The hydrogen bonding configurations are denoted by dashed lines in Figure 11 and the corresponding H-bonding lengths are listed in Table 3. In general the X-H...B H-bonding length is longer than that of corresponding individual monomers. Once the H-bonding has become shortened it strengthens the complex.

#### TD-DFT Results:

To further support the experimental observations of the host-anion interactions and to provide a better insight into fundamental H-bonded cavity and anions binding interaction, TD-DFT calculations were carried out. The HOMO-LUMO and TD-DFT results are listed in Table 4. The B3LYP optimized structure of Host... $H_2PO_4^-$  complex and its electronic delocalization of the frontier molecular orbitals (FMOs) can be seen in Figure 12. We predicted that the addition of anions might change the electronic distribution such that the HOMO is corresponding to the anthracene part and the LUMO corresponding to the anions interaction of the pyrazole parts. Indeed, we found this to be the case as shown in Figure 12 and Figure S6 (a-d). These definitive observations are consistent with the above <sup>1</sup>H NMR measurements. Moreover, to provide the extended conjugations in the current system we employed the DFT and TD-DFT calculations. The predicted absorption wavelengths,

oscillator strength ( $f$ ) and the configuration description of the singlet excited states are shown in Table 4. The energy minimized Host...anion complexes ( $\text{Br}^-$ ,  $\text{Cl}^-$  and  $\text{HSO}_4^-$ ) and its electronic delocalization of the frontier molecular orbitals (FMOs) can be seen in Figure S6 (b-d).

**Table 4.** Calculated HOMO, LUMO, HOMO-LUMO Gap (HLG), Wavelength ( $\lambda_{\text{abs}}$ ) and Oscillator Strength ( $f$ ) for Ho... $\text{H}_2\text{PO}_4^-$ , Ho... $\text{Br}^-$ , Ho... $\text{Cl}^-$  and Ho... $\text{HSO}_4^-$  complexes in solvent phase.

Complex	TD-DFT calculated data <sup>b</sup>							
	HOMO (eV)	LUMO (eV)	HLG <sup>a</sup> (eV)	E	$\lambda_{\text{abs,cal}}^b$ (nm)	$f^c$	Conf <sup>d</sup>	Wt (%)
Ho... $\text{H}_2\text{PO}_4^-$	-4.47	-2.20	2.27	S1	503	0.0237	H→L	69
Ho... $\text{Br}^-$	-4.53	-2.21	2.32	S1	491	0.0203	H→L	84
Ho... $\text{Cl}^-$	-4.54	-2.21	2.33	S1	489	0.0256	H→L	84
Ho... $\text{HSO}_4^-$	-4.49	-2.21	2.28	S1	499	0.014	H→L	74

<sup>a</sup>HOMO, LUMO, and HOMO-LUMO gaps (HLG) are calculated with the B3LYP/6-31G(d) method. <sup>b</sup>Absorption energies are calculated with the TD-DFT method at the B3LYP/6-31G(d) level. <sup>c</sup>Oscillator strength. <sup>d</sup>H and L stands for the predicted HOMO and LUMO, respectively. Ho stands for Host.

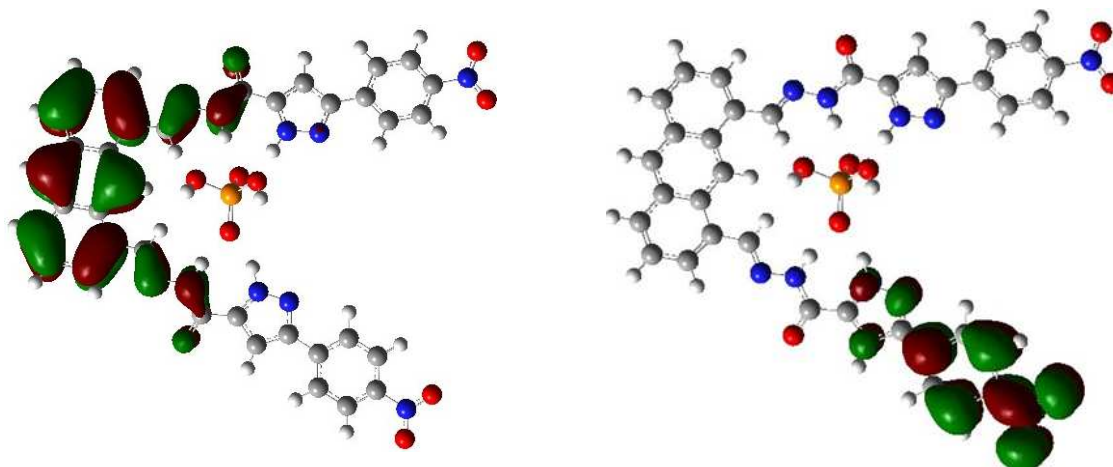


Figure 12. The B3LYP optimized structure of Host...H<sub>2</sub>PO<sub>4</sub><sup>-</sup> complex

For Host-H<sub>2</sub>PO<sub>4</sub><sup>-</sup> anion complex (see Figure 12), the lowest energy singlet transitions are mainly from HOMO to LUMO. For other anion complexes reported here, they also show the similar results as HOMO to LUMO singlet transitions. The HOMO-LUMO gaps (HLG) have also been calculated and reported in Table 4. Among the anions H<sub>2</sub>PO<sub>4</sub><sup>-</sup> showing the lowest HLG supporting the selective binding has confirmed our experimental results. For anthracene and pyrazole both units FMOs are delocalized over the entire structure. To envision the above observations and the trend we carried out the TD-DFT calculations and results are listed in Table 4. In all the anion complexes the transition energies result mainly from HOMO to LUMO.

### Conclusion

In DMSO the H<sub>2</sub>PO<sub>4</sub><sup>-</sup> anion was complexed with presently reported pyrazole containing host via N-H...O and C-H...O types of H-bondings. The pyrazole containing host in the optimized geometry of complex has been interestingly noted as planar, which is not the case in the indole containing host optimized geometry of the complex in our previous report<sup>13</sup>. The

planarity of the host with the  $\text{H}_2\text{PO}_4^-$  anion resulted from four strong N-H...O type and three weak C-H...O type H-bonding. In total seven H-bondings and the planarity of the host in the complex are responsible for the high binding energy. The bond angle of  $\angle\text{N}_{48}\text{H}_{29}\text{O}_{78}$  has been observed to be  $160.9^\circ$  in the complex. The N-H...O type H-bonding appeared to be a strong binding and the C-H...O type H-bonding appears to participate in molecular recognition. From the aforementioned discussions, we concluded that the currently investigated pyrazole containing host has a comparable affinity towards the  $\text{H}_2\text{PO}_4^-$  anion as compared with the previously reported receptor.<sup>13</sup>

### Acknowledgments

This research was supported by the Basic Science Research Program of the Korean National Research Foundation funded by the Korean Ministry of Education, Science and Technology (#2010-0021333).

### Supporting Information

Electronic Supplementary Information (ESI) available:  $^1\text{H}$ ,  $^{13}\text{C}$ , and HRMS spectra and binding energy calculations for the optimized Host-anion complexes.

### References

1. P. A. Furman, J. A. Fyfe, M. H. St. Clair, K. Weinhold, J. L. Rideout, G. A. Freeman, *Proc Natl Acad Sci U S A*, 1986, **83**, 8333-8337.
2. V. Král and J. L. Sessler, *Tetrahedron*, 1995, **51**, 539-554.
3. A. Ojida, Y. Mito-oka, K. Sada and I. Hamachi, *J. Am. Chem. Soc.*, 2004, **126**, 2454-2463.
4. Paul D. Beer, *Chem. Commun.*, 1996, 689-696.
5. L. Fabbrizzi, G. Francese, M. Licchelli, A. Perotti and A. Taglietti, *Chem. Commun.*,

- 1997, 581-582.
6. L. Deng, L. Wang, J. Huo, Q.-H Tan, Q. Yang, H.-J. Yu, H.-Q Gao, and J. F. Wang, *J. Phys. Chem. B* 2008, **112**, 5333-5337.
  7. F. Zapata, A. Caballero, A. Espinosa, A. Tarraga and P. J. Molina, *J. Org. Chem.*, 2008, **73**, 4034-4044.
  8. P. A. Gale, J. R. Hiscock, S. J. Moore, C. Caltagirone, M. B. Hursthouse and M. E. Light, *Chem.–Asian J.*, 2010, **5**, 555–561.
  9. P. A. Gale, J. R. Hiscock, N. Lalaoui, M. E. Light, N. J. Wells and M. Wenzel, *Org. Biomol. Chem.*, 2012, **10**, 5909–5915
  10. S. Kondo and R. Takai, *Org. Lett.*, 2013, **15**, 538-541.
  11. M. S. Wong, P. F. Xia, X. L. Zhang, P. K. Lo, Y.-K. Cheng, K.-T. Yeung, X. Guo, S. Shuang, *J. Org. Chem.* 2005, **70**, 2816-2819.
  12. A. T. Wright, E. V. Anslyn *Org. Lett.*, 2004, **6**, 1341-1344.
  13. T.S. Pandian, S. J. Cho, J. Kang, *J. Org. Chem.*, 2013, **78**, 12121-12127.
  14. D. Wu, F. Jin, W. J. Zhu, C. Li, W. Wang, Y. Tang, H. Jiang, J. Huang, G. Li, Liu, J. *Chem Biol Drug Des.* 2012, **79**, 897-906.
  15. T. Iwasawa, R. J. Hooley, J. Jr. Rebek, *Science*, 2007, **317**, 493-496.
  16. Y. Choi, J. Kang, *J. Incl Phenom Macrocycl*, 2014, **79**, 95-102
  17. S. R. Beeren, J. K. M. Sanders, *Chem. Sci.*, 2011, **2**, 1560-1567
  18. Y.-M. Zhang, Q. Lin, T.-B. Wei, X.-P. Qin, Y. Lin *Chem. Commun.*, 2009, 6074-6076
  19. H. Benesi, H. Hildebrand, *J. Am. Chem. Soc.* 1949, **71**, 2703-2707.
  20. V. Srinivasadesikan, P. K. Sahu, S. H. Lee, *J. Phys. Chem. B* 2012, **116**, 11173-11179.
  21. S. D. Wetmore, R. Schofield, D. M. Smith, L. Radom, *J. Phys. Chem. A* 2001, **105**, 8718-8726.
  22. S. F. Boys, F. Bernardi, *Mol. Phys.* 1970, **19**, 553-566.
  23. A. D. Becke, *Phys. Rev.* 1988, **A38**, 3098-3100.
  24. A. D. Becke, *J. Chem. Phys.* 1993, **98**, 5648-5652.
  25. A. D. Becke, *J. Chem. Phys.* 1997, **107**, 8554.
  26. H. L. Schmider, A. D. Becke *J. Chem. Phys.* 1998, **108**, 9624.
  27. J. Tomasi, B. Mennucci, R. Cammi, *Chem. Rev.* 2005, **105**, 2999-3093.
  28. Gaussian 09, Revision A.02, M. J. Frisch, G. W. Trucks, H. B. Schlegel, G. E.

Scuseria, M. A. Robb, J. R. Cheeseman, G. Scalmani, V. Barone, B. Mennucci, G. A. Petersson, H. Nakatsuji, M. Caricato, X. Li, H. P. Hratchian, A. F. Izmaylov, J. Bloino, G. Zheng, J. L. Sonnenberg, M. Hada, M. Ehara, K. Toyota, R. Fukuda, J. Hasegawa, M. Ishida, T. Nakajima, Y. Honda, O. Kitao, H. Nakai, T. Vreven, J. A. Montgomery, Jr., J. E. Peralta, F. Ogliaro, M. Bearpark, J. J. Heyd, E. Brothers, K. N. Kudin, V. N. Staroverov, R. Kobayashi, J. Normand, K. Raghavachari, A. Rendell, J. C. Burant, S. S. Iyengar, J. Tomasi, M. Cossi, N. Rega, J. M. Millam, M. Klene, J. E. Knox, J. B. Cross, V. Bakken, C. Adamo, J. Jaramillo, R. Gomperts, R. E. Stratmann, O. Yazyev, A. J. Austin, R. Cammi, C. Pomelli, J. W. Ochterski, R. L. Martin, K. Morokuma, V. G. Zakrzewski, G. A. Voth, P. Salvador, J. J. Dannenberg, S. Dapprich, A. D. Daniels, O. Farkas, J. B. Foresman, J. V. Ortiz, J. Cioslowski, D. J. Fox, Gaussian Inc., Wallingford CT, 2009.